Control Engineering Practice 55 (2016) 116–126

Contents lists available at ScienceDirect

Control Engineering Practice

journal homepage: www.elsevier.com/locate/conengprac

Adaptive feedback linearizing control of linear induction motor considering the end-effects

Francesco Alonge [a], Maurizio Cirrincione [b], Filippo D'Ippolito [a], Marcello Pucci [c], Antonino Sferlazza [a,c,*]

[a] D.E.I.M. (Department of Energy Information Engineering and Mathematical Models), Viale delle Scienze, 90128 Palermo, Italy
[b] School of Engineering, University of the South Pacific, Laucala Campus, Suva, Fiji Islands
[c] I.S.S.I.A. C.N.R. Section of Palermo (Institute on Intelligent Systems for Automation), via Dante 12, Palermo 90128, Italy

ARTICLE INFO

Article history:
Received 3 December 2015
Received in revised form
25 June 2016
Accepted 27 June 2016

Keywords:
Linear induction motor
Adaptive systems
Feedback linearization
End-effects
Parameters' estimation

ABSTRACT

This paper proposes an input–output feedback linearization techniques for linear induction motors, taking into consideration the dynamic end-effects. As a main original content, this work proposes a new control law based on the on-line estimation of the induced-part time constant. The estimation law is obtained thanks to a Lyapunov based analysis and thus the stability of the entire control system, including the estimation algorithm, is intrinsically guaranteed. Moreover, with such an approach even the on-line variation of the induced-part time constant with the speed is retrieved, thus improving the behavior of previously developed approaches where such a variation vs. speed is considered a priori known. The proposed control technique, integrating the on-line induced-part time constant estimation, is tested by means of simulations and experiments carried out on a suitably developed test set-up.

© 2016 Elsevier Ltd. All rights reserved.

1. Introduction

A significant amount of research activity has been carried out on Linear Induction Motors (LIMs) since seventies (Boldea & Nasar, 1997, 1999; Laithwaite, 1975; Nasar & Boldea, 1987; Poloujadoff, 1980; Yamamura, 1979). Although they do not require any mechanical apparatus which transform rotating motion in a linear one, a significant increasing of the complexity of their dynamic models occurs, due to the so-called end-effects. These end-effects cause additional significant non-linearities in the LIM dynamic model with that of the Rotating Induction Machine (RIM) (Leonhard, 2001; Vas, 1998).

Since the goal of this work is to propose a high performance control system for the LIM, the dynamic model considered in this paper is that described in Pucci (2014), which takes into account the end-effects. As described in Pucci (2014), these effects produce variations of the electric parameters of the model with the machine speed, and the presence of an additional braking force.

From the other side, the control system theory offers several control techniques to cope with non-linear systems (Isidori, 1995; Khalil, 2002; Slotine & Li, 1991). Among such techniques, the input–output Feedback Linearization (FL) is that of interests for this work.

A restricted number of works in the literature face up to the input–output feedback linearization of LIMs (Huang & Fu, 2003; Lin & Wai, 2001, 2002; Wai & Chu, 2007). All these papers, however, are based on the classic RIM model, as far as the controller design is concerned (De Luca & Ulivi, 1989; Kim, Ha, & Ko, 1990; Krzeminski, 1987; Marino, Peresada, & Valigi, 1993, 2010). It can be thus concluded that the state of the art of the application of FL to LIMs is the same as that of the applications of FL to RIMs, whose current state of the art is described in Marino et al. (2010).

Recently, Alonge, Cirrincione, Pucci, and Sferlazza (2015a, 2015b, 2016) deal with the issue of the input–output FL control of LIM, taking into consideration the LIM additional nonlinearities due to the end-effects in the control action. In particular, in Alonge et al. (2015a, 2015b) it is described by the conventional FL technique that assumes all the known parameters of the motor-load system. However, it is well known that eventual variations of the model parameters can cause deterioration of the behavior of the control system. A first adaptive version of FL is proposed in Alonge et al. (2016), where an adaptation law for the stator resistance is given. In particular an MRAS (Model Reference Adaptive System)

* Corresponding author at: D.E.I.M. (Department of Energy Information Engineering and Mathematical Models), Viale delle Scienze, 90128 Palermo, Italy.
E-mail addresses: francesco.alonge@unipa.it (F. Alonge), m.cirrincione@ieee.org (M. Cirrincione), filippo.dippolito@unipa.it (F. D'Ippolito), pucci@pa.issia.cnr.it (M. Pucci), sferlazza@pa.issia.cnr.it, antonino.sferlazza@unipa.it (A. Sferlazza).

http://dx.doi.org/10.1016/j.conengprac.2016.06.018
0967-0661/© 2016 Elsevier Ltd. All rights reserved.

observer for the stator resistance using a PI-based adaptation law is used. However among all the electrical parameter variations, the induced part time constant variation is certainly one of the most important, since from its correct knowledge depends on the correct field orientation, and to the best Authors' knowledge it has not never been considered in other works in the literature. It should be noted that, while in the RIM, such rotor time constant depends on both the heating/cooling of the rotor and the magnetization level inside the machine (field weakening, optimal efficiency algorithms), in the LIM it also varies with the speed, due to the end-effects.

Starting from these considerations, this paper proposes an adaptive input–output feedback linearization technique for LIMs, taking into consideration the dynamic end-effects. More precisely, as a main original content this work proposes a control law based on the on-line estimation of the induced part time constant. The estimation law is derived from a Lyapunov based approach so as to intrinsically guarantee the stability of the entire control system, including the estimation algorithm. Moreover, with such an approach even the on-line variation of the induced part time constant with the speed is retrieved, with the aim of improving the behavior of the system controlled by the FL described in Alonge et al. (2015a, 2015b, 2016), where the function of the induced part time constant vs. speed is considered a priori known.

2. Dynamic model of the LIM

The main difference between LIMs and RIMs lies in the so-called end-effects. These effects could be divided into two categories: static and dynamic end-effects. Static end-effects are caused by the asymmetric distribution of the reluctances of the magnetic path of the three phases. This kind of effects has not been considered in this paper, even because their presence does not modify significantly the LIM dynamics. On the contrary, dynamic end-effects are caused by the motion of the limited length inductor with a certain speed over an induced part track theoretically of infinite length. Consequently the magnetic flux density in the air-gap varies.

The effect is a deep reduction of the resulting flux in proximity of the entrance and in a deep increase of the flux at the exit of the inductor. This has been taken into consideration in the literature by a so-called end-effect factor Q (Da Silva, Dos Santos, Machado, & De Oliveira, 2003; Duncan, 1983), defined as:

$$Q = \frac{\tau_m}{T_r v}. \tag{1}$$

For the symbols, see Table 1.

As highlighted in Duncan (1983) and Pucci (2014), the higher the machine speed, the higher the air-gap thickness (higher leakage inductance) and the lower the inductor length, the lower the factor Q. It means that the end-effects increase with the machine speed, with the air-gap thickness and reduce with the inductor length. For details to the mathematical modelling of the LIM refer to Pucci (2014).

To the aim of describing the proposal FL technique, the dynamic model of the LIM, taking into consideration its dynamic end-effects (Pucci, 2014), is written in the induced part flux reference frame as in Alonge et al. (2015a) where the input–output FL of LIM is carried out without adaptation of the model parameters. However the model presented in Alonge et al. (2015a) is showed here in a slightly different form in order to make possible the adaptive FL. In particular, writing the equations in the induced part flux reference frame, the following model for the LIM is used:

Table 1
List of symbols.

Symbols	
u_{sx}, u_{sy}	Inductor voltages in the induced part flux reference frame
i_{sx}, i_{sy}	Inductor currents in the induced part flux reference frame
ψ_{rx}, ψ_{ry}	Induced part fluxes in the induced part flux reference frame
f_e	Electromagnetic thrust
f_r	Load force
f_{eb}	Braking force
L_s (L_r)	Inductor (induced part) inductance
L_m	3-Phase magnetizing inductance
R_s (R_r)	Inductor (induced part) resistance
T_r	Induced part time constant
σ	Total leakage factor
ω_r	Electrical angular speed of the induced part
v	Mechanical linear speed
a	Mechanical linear acceleration
p	Pole-pairs
τ_p	Pole-pitch
τ_m	Inductor length
M	Inductor mass

$$\frac{di_{sx}}{dt} = -\frac{R_s}{\hat{\sigma}\hat{L}_s} i_{sx} - \gamma i_{sx} - \hat{L}_m \beta\alpha i_{sx} + \frac{p\pi}{\tau_p} v i_{sy} + \frac{\alpha \hat{L}_m i_{sy}^2}{\psi_r} + \beta\alpha\psi_r + \frac{u_{sx}}{\hat{\sigma}\hat{L}_s}, \tag{2}$$

$$\frac{di_{sy}}{dt} = -\frac{R_s}{\hat{\sigma}\hat{L}_s} i_{sy} - \gamma i_{sy} - \hat{L}_m \beta\alpha i_{sy} - \frac{p\pi}{\tau_p} v i_{sx} - \frac{\alpha \hat{L}_m i_{sy} i_{sx}}{\psi_r} - \beta\frac{p\pi}{\tau_p} v\psi_r + \frac{u_{sy}}{\hat{\sigma}\hat{L}_s}, \tag{3}$$

$$\frac{d\psi_r}{dt} = -(\alpha - \eta)\psi_r + \alpha \hat{L}_m i_{sx}, \tag{4}$$

$$\frac{dv}{dt} = \mu(\psi_r i_{sy}) - \frac{f_r}{M} - \frac{\vartheta}{M}\psi_r^2, \tag{5}$$

where $\psi_r = \psi_{rx}$, and the variables $\alpha, \beta, \gamma, \eta, \mu$ and ϑ are time varying parameters defined as follows:

$$\alpha = \left(\frac{1}{\hat{T}_r} - \frac{\hat{R}_r}{\hat{L}_m}\right), \quad \beta = \frac{\hat{L}_m}{\hat{\sigma}\hat{L}_s\hat{L}_r}, \quad \gamma = \frac{\hat{R}_r}{\hat{\sigma}\hat{L}_s}\left(1 - \frac{\hat{L}_m}{\hat{L}_r}\right), \quad \eta = -\frac{\hat{R}_r}{\hat{L}_m},$$

$$\mu = \frac{3}{2} p \frac{\pi}{\tau_p} \frac{\hat{L}_m}{\hat{L}_r} \frac{1}{M}, \quad \vartheta = \text{sign}(v) \frac{3}{2} \frac{L_r}{\hat{L}_r^2} \frac{1 - e^{-Q}}{p\tau_p},$$

where

$$\hat{L}_m = L_m(1 - f(Q)), \quad \hat{L}_s = L_{\sigma s} + L_m(1 - f(Q)),$$
$$\hat{L}_r = L_{\sigma r} + L_m(1 - f(Q)), \quad \hat{R}_r = R_r f(Q),$$
$$\hat{T}_r = \frac{L_{\sigma r} + L_m(1 - f(Q))}{R_r(1 + f(Q))}, \quad \hat{\sigma} = 1 - \frac{\hat{L}_m^2}{\hat{L}_r \hat{L}_s},$$

with:

$$f(Q) = \frac{1 - e^{-Q}}{Q}. \tag{6}$$

The details for the derivation of model (2)–(4) are not given since it is not the aim of this paper, actually the reader is addressed to Pucci (2014) and Alonge et al. (2015a) for the modelling aspects.

In the following the adaptive feedback linearization procedure based on the above model of LIM will be shown. The adopted linearization approach is inspired to Marino et al. (2010) where it has been developed and applied to the RIM. Here, however, some mathematical issues arising from the suitable definition of the dynamic end-effects will be focused. This will lead to the definition of additional control terms with respect to the RIM case, due to the dynamic end-effects. In fact, different from RIM case, the coefficients α, β, γ, η, μ and the other machine parameters are speed depending and thus time-variant parameters. This will lead to a different feedback law and further interesting considerations compared with RIM model. Moreover, because the on-line estimation is integrated with the FL control law, additional control terms with respect to Alonge et al. (2015a, 2016) arise as well.

3. Adaptive input–output feedback linearization

The goal of this paper is to reconsider the state feedback input–output linearizing control showed in Alonge et al. (2015a) when the parameter α is unknown. To this end, denoting by $\tilde{\alpha}$ the estimate of the parameter α, the corresponding estimation error can be written as follows:

$$e_\alpha = \alpha - \tilde{\alpha}. \tag{7}$$

Now, the two control inputs u_{sx} and u_{sy} are designed through a state feedback as follows:

$$u_{sx} = \hat{\sigma}\hat{L}_s\left(\frac{R_s}{\hat{\sigma}\hat{L}_s}i_{sx} + \gamma i_{sx} + \hat{L}_m\beta\tilde{\alpha}i_{sx} - \frac{p\pi}{\tau_p}vi_{sy} - \frac{\tilde{\alpha}\hat{L}_m i_{sy}^2}{\psi_r} - \beta\tilde{\alpha}\psi_r + \nu_x\right), \tag{8}$$

$$u_{sy} = \hat{\sigma}\hat{L}_s\left(\frac{R_s}{\hat{\sigma}\hat{L}_s}i_{sy} + \gamma i_{sy} + \hat{L}_m\beta\tilde{\alpha}i_{sy} + \frac{p\pi}{\tau_p}vi_{sx} + \frac{\tilde{\alpha}\hat{L}_m i_{sy}i_{sx}}{\psi_r} + \beta\frac{p\pi}{\tau_p}v\psi_r + \nu_y\right), \tag{9}$$

where ν_x and ν_y are additional control inputs that will be designed suitably. Replacing (8) and (9) in the model (2)–(4), the following equations are obtained:

$$\frac{di_{sx}}{dt} = \left(-\hat{L}_m\beta i_{sx} + \frac{\hat{L}_m i_{sy}^2}{\psi_r} + \beta\psi_r\right)e_\alpha + \nu_x, \tag{10}$$

$$\frac{di_{sy}}{dt} = \left(-\hat{L}_m\beta i_{sy} - \frac{\hat{L}_m i_{sx}i_{sy}}{\psi_r}\right)e_\alpha + \nu_y, \tag{11}$$

$$\frac{d\psi_r}{dt} = -(\alpha-\eta)\psi_r + \alpha\hat{L}_m i_{sx}, \tag{12}$$

$$\frac{dv}{dt} = \mu(\psi_r i_{sy}) - \frac{f_r}{M} - \frac{\vartheta}{M}\psi_r^2. \tag{13}$$

As can be see from model (10)–(13), the speed and flux dynamics are not never decoupled. This is another difference between RIM and LIM, indeed in the RIM case the decoupling between speed and flux works when the machine works at constant flux and $\tilde{\alpha} = \alpha$, but in this case even in these conditions the decoupling is not achieved. So to overcome this problem, and to obtain a fully decoupled linear model, a further state feedback loop is necessary.

Let us define a new state variable $a = \frac{dv}{dt}$ called *linear acceleration*, in place of i_{sy} as a new state variable:

$$a = \mu(\psi_r i_{sy}) - \frac{f_r}{M} - \frac{f_{eb}}{M}. \tag{14}$$

If the load thrust variation is assumed to be sufficiently slow, i.e. $\dot{f}_r \approx 0$, then the derivate of a can be written as follows:

$$\frac{da}{dt} = \left(\mu i_{sy} + \frac{2\theta}{M}\psi_r\right)\left(\alpha\hat{L}_m i_{sx} - (\alpha-\eta)\psi_r\right) - \frac{\dot{\theta}}{M}\psi_r^2 - \mu\hat{L}_m i_{sy}(i_{sx} + \beta\psi_r)e_\alpha + \mu\psi_r\nu_y. \tag{15}$$

In order to compute (15), the assumption $\dot{\mu} \approx 0$ has been considered. Actually this approximation is a realistic assumption since μ is the ratio between two time varying terms ($\hat{L}_r$ and $\hat{L}_m$), which vary with the same function $1 - f(Q)$. So μ is approximatively a constant.

If the control input ν_y is defined as:

$$\nu_y = \frac{\left(\mu i_{sy} + \frac{2\theta}{M}\psi_r\right)}{\mu}\left((\tilde{\alpha}-\eta) - \frac{\tilde{\alpha}\hat{L}_m i_{sx}}{\psi_r}\right) + \frac{\dot{\theta}}{M\mu}\psi_r + \frac{1}{\mu\psi_r}\nu_y', \tag{16}$$

then the derivative of the acceleration (15) becomes:

$$\frac{da}{dt} = -\left(\mu i_{sy}(1 + \beta\hat{L}_m) + \frac{2\theta}{M}(\psi_r - \hat{L}_m i_{sx})\right)\psi_r e_\alpha + \nu_y'. \tag{17}$$

As for the acceleration, a further new state variable $\tilde{\nu}_\psi = \left.\frac{d\psi_r}{dt}\right|_{\alpha=\tilde{\alpha}}$ has been introduced, in place of i_{sx}:

$$\tilde{\nu}_\psi = -(\tilde{\alpha}-\eta)\psi_r + \tilde{\alpha}\hat{L}_m i_{sx}. \tag{18}$$

Using (18), Eq. (12) can be written as:

$$\frac{d\psi_r}{dt} = \tilde{\nu}_\psi + \left(\hat{L}_m i_{sx} - \psi_r\right)e_\alpha. \tag{19}$$

Computing the derivative of (18), the following is obtained:

$$\frac{d\tilde{\nu}_\psi}{dt} = \dot{\tilde{\alpha}}\left(\hat{L}_m i_{sx} - \psi_r\right) + \dot{\eta}\psi_r + \tilde{\alpha}\dot{\hat{L}}_m i_{sx} - (\tilde{\alpha}-\eta)\left(\alpha\hat{L}_m i_{sx} - (\alpha-\eta)\psi_r\right) + \tilde{\alpha}\hat{L}_m\left(\left(\beta\psi_r + \frac{\hat{L}_m i_{sy}^2}{\psi_r} - \hat{L}_m\beta i_{sx}\right)e_\alpha + \nu_x\right). \tag{20}$$

If the control input ν_x is defined as:

$$\nu_x = -\frac{1}{\tilde{\alpha}\hat{L}_m}\left(\dot{\tilde{\alpha}}\left(\hat{L}_m i_{sx} - \psi_r\right) + \dot{\eta}\psi_r + \tilde{\alpha}\dot{\hat{L}}_m i_{sx}\right) + (\tilde{\alpha}-\eta)i_{sx} - \frac{(\tilde{\alpha}-\eta)^2}{\tilde{\alpha}\hat{L}_m}\psi_r + \frac{1}{\tilde{\alpha}\hat{L}_m}\nu_x', \tag{21}$$

then the derivative of $\tilde{\nu}_\psi$ (20) becomes:

$$\frac{d\tilde{\nu}_\psi}{dt} = \left((\tilde{\alpha}-\eta + \tilde{\alpha}\beta\hat{L}_m)(\psi_r - \hat{L}_m i_{sx}) + \frac{\tilde{\alpha}\hat{L}_m^2 i_{sy}^2}{\psi_r}\right)e_\alpha + \nu_x'. \tag{22}$$

Finally using (17) and (22) and computing the control input ν_y and ν_x as in (16) and (21), respectively, the model (10)–(13) can be written in terms of the state variables (ψ_r, $\tilde{\nu}_\psi$, v, a) as follows:

$$\frac{d\psi_r}{dt} = \left(\hat{L}_m i_{sx} - \psi_r\right)e_\alpha + \tilde{\nu}_\psi, \tag{23}$$

$$\frac{d\tilde{\nu}_{\psi}}{dt} = \left(\left(\tilde{\alpha} - \eta + \tilde{\alpha}\beta\hat{L}_m\right)\left(\psi_r - \hat{L}_m i_{sx}\right) + \frac{\tilde{\alpha}\hat{L}_m^2 i_{sy}^2}{\psi_r} \right) e_{\alpha} + \nu_x', \tag{24}$$

$$\frac{dv}{dt} = a, \tag{25}$$

$$\frac{da}{dt} = -\left(\mu i_{sy}(1 + \beta\hat{L}_m) + \frac{2\theta}{M}(\psi_r - \hat{L}_m i_{sx}) \right) \psi_r e_{\alpha} + \nu_y'. \tag{26}$$

As can be easily see from (23)–(26), if the parameter α is perfectly known, then $e_{\alpha} = 0$ and the perfect input–output feedback linearization of LIM, considering the end-effects, is achieved (Alonge et al., 2015a, Eqs. (46)–(49)). However if the parameter α is unknown the following theorem permits us to obtain an adaptation law for α and a contemporary control law such that $e_{\alpha} \to 0$ (consequently the input–output feedback linearization will be achieved). At the same time, the tracking errors of both speed and flux are governed to zero.

To this aim the following tracking error vectors are introduced:

$$\boldsymbol{\zeta}_v = \begin{bmatrix} v - v_{ref} \\ a - a_{ref} \end{bmatrix}, \quad \boldsymbol{\zeta}_{\psi} = \begin{bmatrix} \psi_r - \psi_{r_{ref}} \\ \tilde{\nu}_{\psi} - \nu_{\psi_{ref}} \end{bmatrix}, \tag{27}$$

where v_{ref}, a_{ref}, $\psi_{r_{ref}}$ and $\nu_{\psi_{ref}}$ are respectively the reference values of speed, acceleration, induced part flux, and derivative of the induced part flux. Now the following result can be given:

Theorem 1. *Let us assume that the input signals ν_x' and ν_y' are designed as:*

$$\nu_x' = -\begin{bmatrix} k_{\psi 1} & k_{\psi 2} \end{bmatrix} \boldsymbol{\zeta}_{\psi} + \frac{d^2\psi_{r_{ref}}}{dt^2}, \tag{28}$$

$$\nu_y' = -\begin{bmatrix} k_{v1} & k_{v2} \end{bmatrix} \boldsymbol{\zeta}_v + \frac{d^2 v_{ref}}{dt^2}, \tag{29}$$

for some positive constant design parameters $k_{\psi 1}$, $k_{\psi 2}$, k_{v1} and k_{v2}, and let us assume that the adaptation law for parameter α is chosen as follows:

$$\dot{\tilde{\alpha}} = \sigma_{\alpha} \left(-\boldsymbol{\zeta}_v^T \boldsymbol{P}_v \begin{bmatrix} 0 \\ \left(\mu i_{sy}(1 + \beta\hat{L}_m) + \frac{2\theta}{M}(\psi_r - \hat{L}_m i_{sx}) \right) \psi_r \end{bmatrix} + \boldsymbol{\zeta}_{\psi}^T \boldsymbol{P}_{\psi} \begin{bmatrix} \hat{L}_m i_{sx} - \psi_r \\ \left(\tilde{\alpha} - \eta + \tilde{\alpha}\beta\hat{L}_m \right)\left(\psi_r - \hat{L}_m i_{sx} \right) + \frac{\tilde{\alpha}\hat{L}_m^2 i_{sy}^2}{\psi_r} \end{bmatrix} \right), \tag{30}$$

for some $\sigma_{\alpha} > 0$, and for some positive definite matrices $\boldsymbol{P}_v$ and $\boldsymbol{P}_{\psi}$ designed as follows:

$$\boldsymbol{P}_v = \frac{1}{2k_{v1}k_{v2}} \begin{bmatrix} k_{v1}^2 + k_{v1} + k_{v2}^2 & k_{v2} \\ k_{v2} & k_{v1} + 1 \end{bmatrix}, \tag{31}$$

$$\boldsymbol{P}_{\psi} = \frac{1}{2k_{\psi 1}k_{\psi 2}} \begin{bmatrix} k_{\psi 1}^2 + k_{\psi 1} + k_{\psi 2}^2 & k_{\psi 2} \\ k_{\psi 2} & k_{\psi 1} + 1 \end{bmatrix}. \tag{32}$$

Then denoting the error $\boldsymbol{e} = \begin{bmatrix} \boldsymbol{\zeta}_v^T & \boldsymbol{\zeta}_{\psi}^T & e_{\alpha} \end{bmatrix}^T$, the quadratic positive definite Lyapunov function:

$$V(\boldsymbol{e}) = \boldsymbol{e}^T \begin{bmatrix} \boldsymbol{P}_v & \boldsymbol{0}_{2\times 2} & \boldsymbol{0}_{2\times 1} \\ \boldsymbol{0}_{2\times 2} & \boldsymbol{P}_{\psi} & \boldsymbol{0}_{2\times 1} \\ \boldsymbol{0}_{1\times 2} & \boldsymbol{0}_{1\times 2} & \sigma_{\alpha} \end{bmatrix} \boldsymbol{e}, \tag{33}$$

satisfies:

$$\dot{V}(\boldsymbol{e}) = \left\langle \nabla V(\boldsymbol{e}), \dot{\boldsymbol{e}} \right\rangle = -\| \boldsymbol{\zeta}_v \|^2 - \| \boldsymbol{\zeta}_{\psi} \|^2 < 0. \tag{34}$$

along all solutions to (23)–(26), (30).

Proof. First of all note that the symmetric matrices P_{ψ} and P_v are effectively positive definite because $k_{\psi 1} > 0$, $k_{\psi 2} > 0$, $k_{v1} > 0$ and $k_{v2} > 0$, therefore their upper-left and down-right entries are clearly positive and their determinants satisfy $\frac{k_{v1}^2 + 2k_{v1} + k_{v2}^2 + 1}{2k_{v2}} > 0$ and $\frac{k_{\psi 1}^2 + 2k_{\psi 1} + k_{\psi 2}^2 + 1}{2k_{\psi 2}} > 0$, so (33) is an effectively candidate Lyapunov function. Computing the derivative of V along all solutions to (23)–(26), (30), and considering that ν_x' and ν_y' are designed as in (28) and (29), respectively, it is obtained:

$$\begin{aligned} \dot{V}(\boldsymbol{e}) = {} & 2\boldsymbol{\zeta}_v^T \boldsymbol{P}_v \dot{\boldsymbol{\zeta}}_v + 2\boldsymbol{\zeta}_{\psi}^T \boldsymbol{P}_{\psi} \dot{\boldsymbol{\zeta}}_{\psi} + 2\frac{e_{\alpha}}{\sigma_{\alpha}} \dot{e}_{\alpha} = 2\boldsymbol{\zeta}_v^T \boldsymbol{P}_v \begin{bmatrix} 0 & 1 \\ -k_{v1} & -k_{v2} \end{bmatrix} \boldsymbol{\zeta}_v + 2\boldsymbol{\zeta}_{\psi}^T \boldsymbol{P}_{\psi} \begin{bmatrix} 0 & 1 \\ -k_{\psi 1} & -k_{\psi 2} \end{bmatrix} \boldsymbol{\zeta}_{\psi} \\ & - 2\boldsymbol{\zeta}_v^T \boldsymbol{P}_v \begin{bmatrix} 0 \\ \left(\mu i_{sy}(1 + \beta\hat{L}_m) + \frac{2\theta}{M}(\psi_r - \hat{L}_m i_{sx}) \right) \psi_r \end{bmatrix} e_{\alpha} \\ & + 2\boldsymbol{\zeta}_{\psi}^T \boldsymbol{P}_{\psi} \begin{bmatrix} \hat{L}_m i_{sx} - \psi_r \\ \left(\tilde{\alpha} - \eta + \tilde{\alpha}\beta\hat{L}_m \right)\left(\psi_r - \hat{L}_m i_{sx} \right) + \frac{\tilde{\alpha}\hat{L}_m^2 i_{sy}^2}{\psi_r} \end{bmatrix} e_{\alpha} + 2\frac{e_{\alpha}}{\sigma_{\alpha}}(\dot{\alpha} - \dot{\tilde{\alpha}}) \\ & . \end{aligned} \tag{35}$$

If $\dot{\tilde{\alpha}}$ is chosen as in (30) the third and the fourth terms in (35) are cancelled from the last term $-2\frac{e_{\alpha}}{\sigma_{\alpha}}\dot{\tilde{\alpha}}$. Moreover it is assumed that the parameter α keeps constant during the adaptation period. As it is well known this is a common assumption in the adaptive systems (Landau, Lozano, & Karimi, 2011). This assumption is further supported since usually the LIMs are controlled in order to maintain a constant speed (constant speed means constant parameter α). Moreover during the transients, since the speed is a mechanical variable, the speed variations are slower than the convergence speed of $\tilde{\alpha}$ that can be increased acting on the parameter σ_{α}. This is particularly true for a LIM where the maximum acceleration is always quite limited because of the heavy moving inductor.

Under this considerations the derivative of V in (35) becomes:

$$\dot{V}(\boldsymbol{e}) = 2\boldsymbol{\zeta}_v^T \boldsymbol{P}_v \begin{bmatrix} 0 & 1 \\ -k_{v1} & -k_{v2} \end{bmatrix} \boldsymbol{\zeta}_v + 2\boldsymbol{\zeta}_{\psi}^T \boldsymbol{P}_{\psi} \begin{bmatrix} 0 & 1 \\ -k_{\psi 1} & -k_{\psi 2} \end{bmatrix} \boldsymbol{\zeta}_{\psi}. \tag{36}$$

Computing the symmetric part of $\boldsymbol{P}_v \begin{bmatrix} 0 & 1 \\ -k_{v1} & -k_{v2} \end{bmatrix}$ and $\boldsymbol{P}_{\psi} \begin{bmatrix} 0 & 1 \\ -k_{\psi 1} & -k_{\psi 2} \end{bmatrix}$ for $\boldsymbol{P}_v$ and $\boldsymbol{P}_{\psi}$ as in (31) and (32), respectively, since their skew-symmetric parts do not give any contribution to the quadratic form, the following is obtained:

$$\frac{1}{2}\left(\boldsymbol{P}_v \begin{bmatrix} 0 & 1 \\ -k_{v1} & -k_{v2} \end{bmatrix} + \begin{bmatrix} 0 & 1 \\ -k_{v1} & -k_{v2} \end{bmatrix}^T \boldsymbol{P}_v \right) = -\frac{\boldsymbol{I}_{2\times 2}}{2}, \tag{37}$$

$$\frac{1}{2}\left(\boldsymbol{P}_{\psi}\begin{bmatrix}0 & 1\\ -k_{\psi 1} & -k_{\psi 2}\end{bmatrix}+\begin{bmatrix}0 & 1\\ -k_{\psi 1} & -k_{\psi 2}\end{bmatrix}^{T}\boldsymbol{P}_{\psi}\right)=-\frac{\boldsymbol{I}_{2\times 2}}{2}. \tag{38}$$

(Recall that the symmetric part of a generic matrix $\boldsymbol{A}$ is $\frac{\boldsymbol{A}^T+\boldsymbol{A}}{2}$).

In conclusion, under the particular choice of $\boldsymbol{P}_v$ and $\boldsymbol{P}_{\psi}$ as in (31) and (32), respectively, (36) becomes:

$$\dot{V}(\boldsymbol{e})=-\boldsymbol{\xi}_v^T\boldsymbol{I}_{2\times 2}\boldsymbol{\xi}_v-\boldsymbol{\xi}_{\psi}^T\boldsymbol{I}_{2\times 2}\boldsymbol{\xi}_{\psi}=-\|\boldsymbol{\xi}_v\|^2-\|\boldsymbol{\xi}_{\psi}\|^2. \tag{39}$$

This concludes the proof. □

Remark 1. It is useful to note that this adaptation law works only when speed and/or flux tracking errors occur. Actually, until $\|\boldsymbol{\xi}_v\|=\|\boldsymbol{\xi}_{\psi}\|=0$, then $\dot{\tilde{\alpha}}=0$, so the adapted parameter keeps constant also if it is wrong and $e_{\alpha}\neq 0$, but if the speed or flux reference varies then the algorithm acts in order to bring to zero the tracking error together with error on α. This fact is evident from the proof of the theorem and will be showed also in the experimental results in the last section of this work. Sometimes the assumption of persistent excitation is done in order to avoid this common problem in the adaptive systems.

Remark 2. It must be noted that, according to the strong nonlinear nature of the LIM model, the $\hat{T}_r$ parameter cannot be directly estimated, actually the parameter α has been estimated. However the parameter α is equal to the difference between $\frac{1}{\hat{T}_r}$ and $\frac{\hat{R}_r}{\hat{L}_m}$ which can be approximated with good accuracy with $\frac{1}{\hat{T}_r\left(2+\frac{1}{f(Q)}\right)}$. Therefore the subtractive term in α depending on the LIM speed is much lower than $\frac{1}{\hat{T}_r}$. This justifies the fact that the α estimate is a good estimate of $\hat{T}_r$.

4. Simulation results

The proposed adaptive FL control technique taking into consideration the LIM dynamic end-effects, with integrated on-line estimation of the parameter α, has been tested in both numerical simulation and experimentally. The aim of the numerical simulations is to show some important results, among which the coherence between simulation and experiments. Moreover, some tests can be made only in numerical simulation because of constraints of the experimental set-up. This is the case of high speed (rated speed of about 5 m/s) tests. As a matter of fact, such test cannot be made experimentally because of the limited length of the induced part track (1.6 m). For this reason the high speed test has been carried out by simulation, and the tests at lower speed have been carried out both experimentally and by means of simulations in order to compare with the obtained experimental results. A further scope of adopting numerical simulation is to prove the effectiveness of the proposed approach; in fact, by means of simulations it is possible to show the convergence of the adaptation algorithm of the induced-part time constant as well as its accuracy in the estimation. On the contrary, it cannot be done experimentally due to the fact that the induced-part time is unknown and unmeasurable.

Numerical simulations have been performed in Matlab® – Simulink®environment. With this regard, the dynamic model of the LIM including its end-effect, the adaptive FL control technique, the flux model and the inverter model controlled by its SV-PWM (Space-Vector Pulse-Width Modulation) technique, have been purposely developed. With regard to the LIM dynamic model used as “machine under test”, the model proposed and validated in Pucci (2014) both by means of finite element analysis and experimentally has been adopted.

To demonstrate the advantages of the adoption of the proposed adaptive FL, it has been compared to the FL control technique proposed in Alonge et al. (2015b), which does not present any robustness versus any parameters' variation. As a matter of fact, whenever the α estimation feature is not activated by the control system occurring when the estimated $\tilde{\alpha}$ coincides with the corresponding one of the LIM, the proposed FL coincides with Alonge et al. (2015b).

The first test consists in a speed step from 0 to 5 m/s ($t=1$ s) followed by a speed reversal 5 to -5 m/s ($t=5$ s) at no load. Contemporary to the first speed step, a $t=1$ s, a $|\psi_r|$ step variation from 0 to 0.6 Wb (rated flux) is commanded. The LIM has been operated so that, at the beginning, the value of $\tilde{\alpha}$ provided to the FL controller is twice the value of the real machine (detuning of the FL controller) which is a very challenging working condition, very rarely encountered in the real world practice. It should be further noted that, in such tests, the flux model used to estimate $|\psi_r|$ is adapted on-line coherently with the FL controller, in accordance with the current estimation of α. Fig. 1 shows the reference and real speed, speed tracking error during such a test. Fig. 2 shows the corresponding waveforms of the reference and real $|\psi_r|$, flux tracking error, Fig. 3 shows the corresponding waveforms of the i_{sx}, i_{sy} inductor currents and, finally, Fig. 4 shows the corresponding waveforms of the reference and estimated $\tilde{\alpha}$, as well as the estimation tracking error. The figure of the estimated $\tilde{\alpha}$ clearly highlights that the FL controller is initially completely detuned as far as the knowledge of such parameter is concerned. After $t=1$ s, when the first speed step reference occurs, the estimated $\tilde{\alpha}$ correctly tracks the real one of the machine; correspondingly its estimation errors converge to zero. It should be noted that the algorithm is able to track the correct value of the parameter, starting from its wrong knowledge, even if the real parameter varies during the estimation process. This is a peculiarity of such a technique when applied to the LIM case, because L_r varies with the machine speed because of the dynamic end-effects independently from the magnetizing level of the machine. Such a complication does not exist in the RIM case, where L_r can be assumed to be constant independently from the speed if the flux level is maintained constant. Coherently with the $\tilde{\alpha}$ adaptation law in (30), the estimated parameter is adapted on-line only in the presence of alternatively a flux tracking error or in the presence of a load. When the speed reversal occurs, at $t=5$ s, the estimated $\tilde{\alpha}$ tend to track

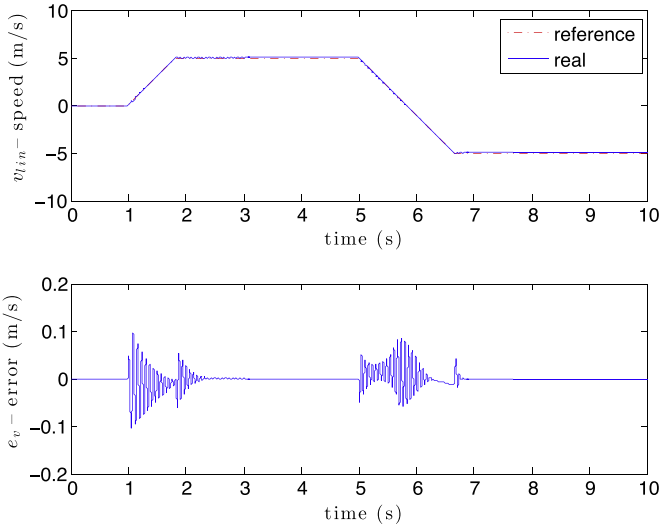

Fig. 1. Reference and real speed, speed tracking error during a speed step 0 → 5 m/s followed by a speed reversal 5 → – 5 m/s at no load (simulation).

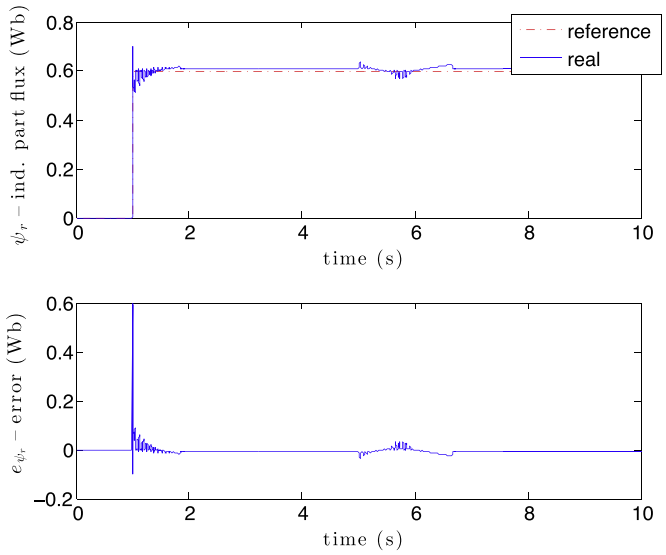

Fig. 2. Reference and real flux $|\psi_r|$, flux tracking error during a speed step 0 → 5 m/s followed by a speed reversal 5 → – 5 m/s at no load (simulation).

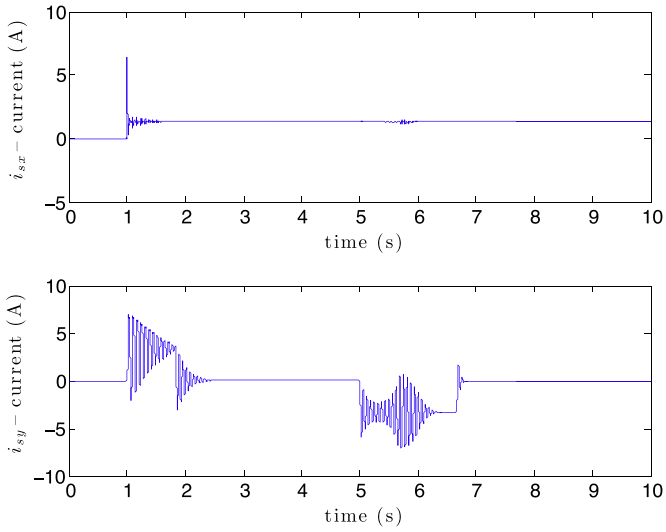

Fig. 3. i_{sx}, i_{sy} inductor currents during a speed step 0 → 5 m/s followed by a speed reversal 5 → – 5 m/s at no load (simulation).

the real one, but its dynamics is slower than that of the real parameter, which is governed by the speed loop dynamic. During the speed transient, the controller is thus only partially tuned, while at the end of the transient the estimated $\tilde{\alpha}$ converges to the real value of the machine. It should be further noted that differently from Alonge et al. (2015b) and Pucci (2012) where the variation law of the L_m with the speed had been assumed correctly modelled and known a priori (with the related approximations), here such a variation is estimated on-line. This is a particularly interesting characteristics of such an approach, different from that in Alonge et al. (2015a, 2015b) where the variation law of the parameters versus the LIM speed had been assumed perfectly a priori known. As a matter of fact, however, the above mentioned variation law, even if well approximated, presents some limits. Such limits are overcome here thanks to the on-line estimation of the variability of such parameters with the LIM speed.

Correspondingly, Fig. 1 shows that the FL controller permits us to suitably control the speed during the entire test, with the speed tracking error converging to zero quickly at the end of each speed transient. Same considerations can be made for the $|\psi_r|$ waveform,

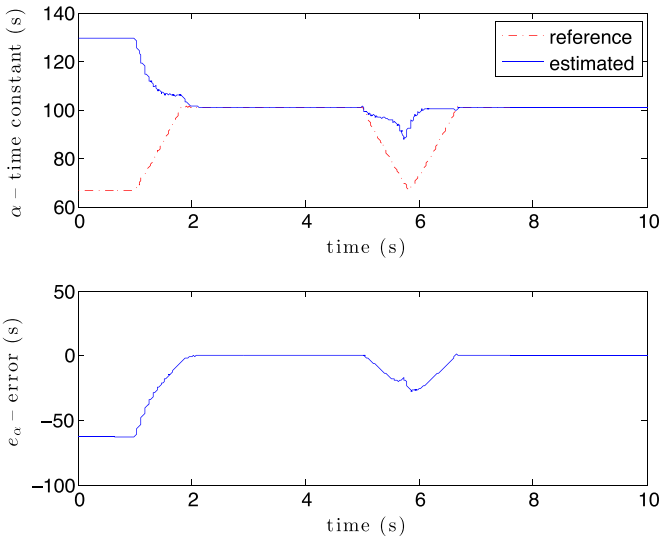

Fig. 4. Reference α and estimated $\tilde{\alpha}$, estimation tracking error during a speed 0 → 5 m/s followed by a speed reversal step 5 → – 5 m/s at no load (simulation).

which correctly tracks its reference with zero steady-state tracking error, thanks to the on-line $\tilde{\alpha}$ estimation feature. Coherently with what stated above, the flux presents a non-null tracking error during speed transient, caused by the variation of L_r with the LIM speed which is estimated on-line, and not a priori established as in Alonge et al. (2015b) and Pucci (2012). Finally, the i_{sx}, i_{sy} waveforms are coherent with the speed and flux waveforms. In particular, i_{sx} is maintained at a constant value, because the magnetization level of the machine is maintained constant. On the other hand, i_{sy} exhibits step-wise waveform, which is proportional to the electromagnetic force. It must be noted that, during the speed transients, i_{sy} presents some oscillations. Such oscillations are caused by the fact that $\tilde{\alpha}$ presents a non-null estimation error during transients, causing a non-perfect field orientation during transients, caused by the LIM end-effects.

Figs. 5–8 show the same kind of waveforms, obtained under constant LIM speed operation set at 5 m/s and constant induced part flux amplitude set at 0.6 Wb. The LIM is initially operated at no-load, while at $t=5$ s a load step load force of amplitude 80 N is applied. As in the first test, the LIM has been operated so that, at the beginning, the value of $\tilde{\alpha}$ provided to the FL controller is twice the value of the real machine (detuning of the FL controller). Fig. 8 clearly highlights that, coherently with the $\tilde{\alpha}$ adaptation law in (30), the estimated parameter is adapted on-line only in the presence of the application of the load force. During the first 5 s, at no load conditions, the FL controller remains detuned. On the contrary, at $t=5$ s, the estimated $\tilde{\alpha}$ converges quickly towards its real value, guaranteeing the correct field orientation conditions. At the same time, the speed waveform exhibits a very fast dynamics, with a peak value of speed tracking error which is very limited, even during the contemporary convergence process of $\tilde{\alpha}$. Even the $|\psi_r|$ waveform correctly tracks its reference with zero steady-state tracking error, thanks to the on-line $\tilde{\alpha}$ estimation feature.

Finally, the i_{sx}, i_{sy} waveforms are coherent with the speed and flux waveforms. In particular, i_{sx} is maintained at a constant value, because the magnetization level of the machine is maintained constant. On the other hand, i_{sy} exhibits a step-wise waveform, which is proportional to the electromagnetic force. As recalled above for the first test, during the speed transients, i_{sy} presents some oscillations, whose interpretation has already been given above.

Finally, as last test, Figs. 9–12 show the same kind of waveforms, obtained during a low speed test. Such a test is exactly the same performed experimentally, whose results are shown in Figs. 17–20. At $t=1$ s a step reference of the induced part flux of

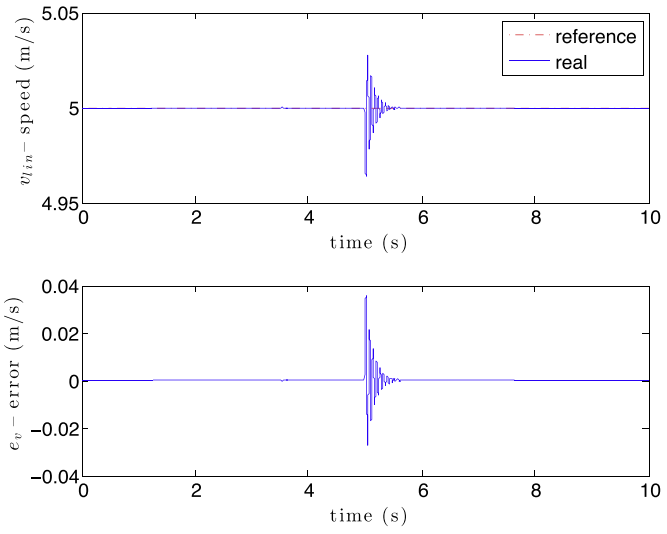

Fig. 5. Reference and real speed, speed tracking error with $v=5$ m/s, $|\psi_r|=0.6$ Wb when a step load force equal to 80 N is applied (simulation).

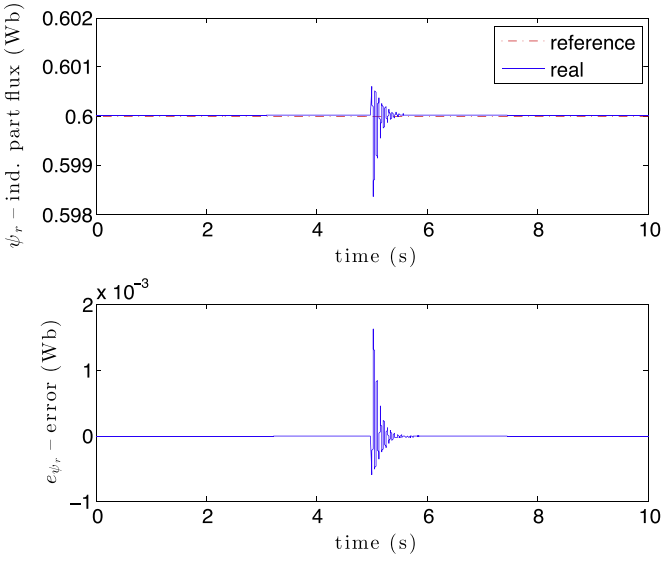

Fig. 6. Reference and real flux $|\psi_r|$, flux tracking error with $v=5$ m/s, $|\psi_r|=0.6$ Wb when a step load force equal to 80 N is applied (simulation).

0.6 Wb has been given to the drive. At $t=2.5$ s a speed step reference of 0.2 m/s has been given at no load. As in the previous tests, at the beginning, the value of $\tilde{\alpha}$ provided to the FL controller is different from the value of the real machine. Fig. 12 clearly highlights that, coherently with the $\tilde{\alpha}$ adaptation law in (30), the estimated parameter is adapted on-line firstly during the initial flux transient and secondly during the speed transient. The speed waveform exhibits a very fast dynamics, even during the contemporary convergence process of $\tilde{\alpha}$. Even the $|\psi_r|$ waveform, shown in Fig. 10, correctly tracks its reference with zero steady-state tracking error, thanks to the on-line $\tilde{\alpha}$ estimation feature. Finally, the i_{sx}, i_{sy} waveforms, shown on Fig. 11, are coherent with the speed and flux waveforms. In particular, i_{sx} is maintained at a constant value, because the magnetization level of the machine is maintained constant. On the other hand, i_{sy} exhibits a step-wise waveform, which is proportional to the electromagnetic force.

With the aim of showing the improvements achievable thanks to the adoption of the proposed adaptive FL taking into consideration the LIM end-effects compared to the non-adaptive FL, Fig. 13(a) and (b) shows, respectively, the surfaces of the speed and

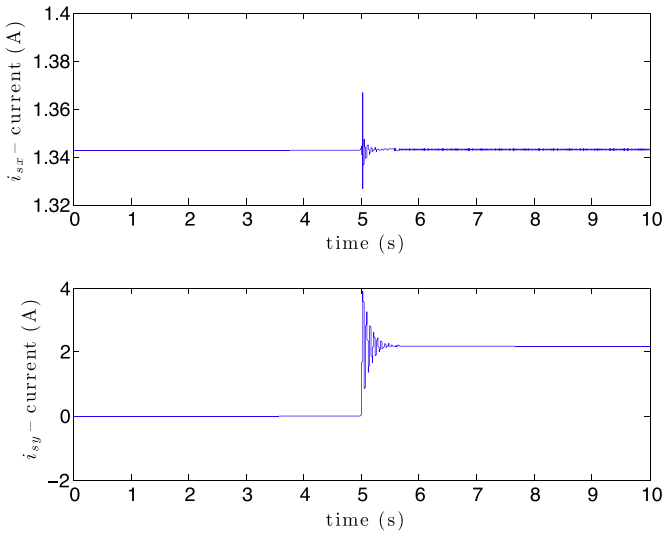

Fig. 7. i_{sx}, i_{sy} inductor currents with $v=5$ m/s, $|\psi_r|=0.6$ Wb when a step load force equal to 80 N is applied (simulation).

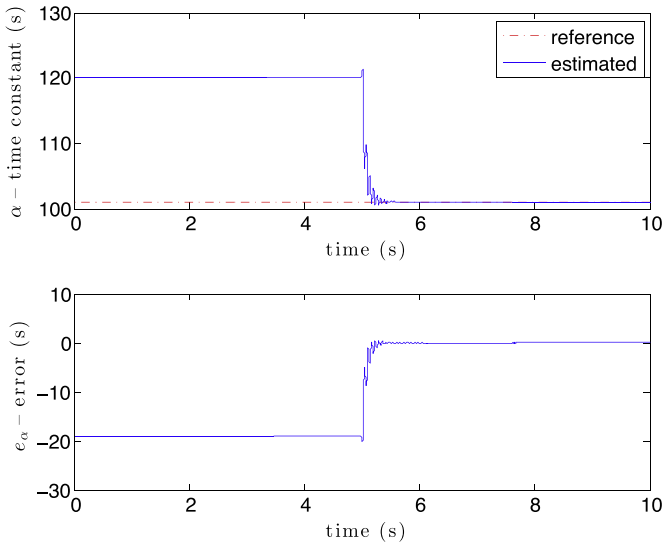

Fig. 8. Reference α and estimated $\tilde{\alpha}$, estimation tracking error with $v=5$ m/s, $|\psi_r|=0.6$ Wb when a step load force equal to 80 N is applied (simulation).

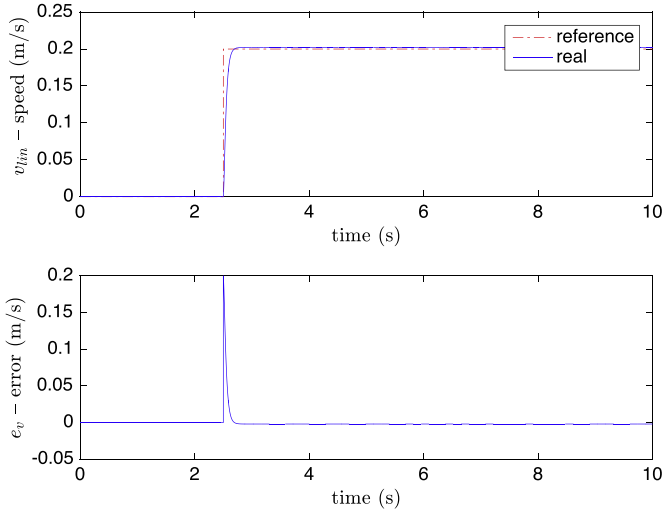

Fig. 9. Reference and real speed, speed tracking error with a flux step of 0.6 Wb at $t=1$ s, followed by a speed step $0 \rightarrow 0.2$ m/s at no load (simulation).

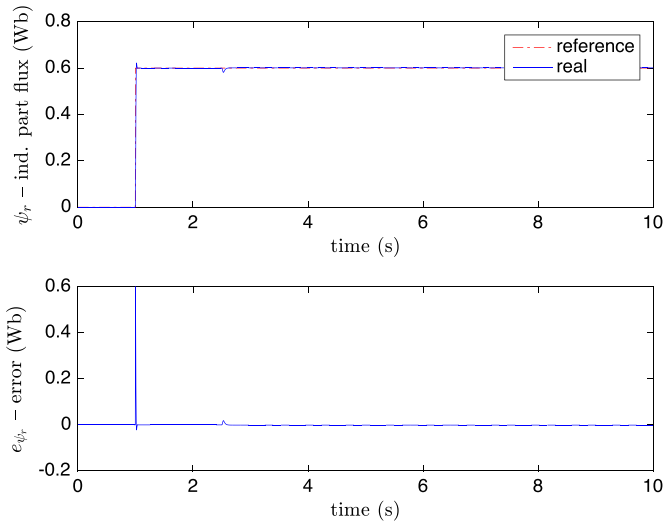

Fig. 10. Reference and real flux $|\psi_r|$, flux tracking error with a flux step of 0.6 Wb at $t=1$ s, followed by a speed step $0 \rightarrow 0.2$ m/s at no load (simulation).

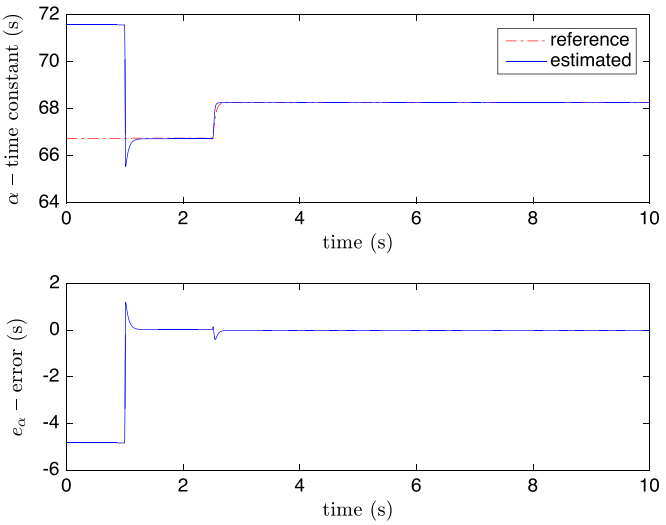

Fig. 12. Reference α and estimated $\tilde{\alpha}$, estimation tracking error with a flux step of 0.6 Wb at $t=1$ s, followed by a speed step $0 \rightarrow 0.2$ m/s at no load (simulation).

flux tracking errors versus LIM speed and load force, obtained with the non-adaptive FL for $\tilde{\alpha} = 0.5\alpha$ (upper plots) and $\tilde{\alpha} = 0.75\alpha$ (lower plots) (a), and for $\tilde{\alpha} = 1.25\alpha$ (upper plots) and $\tilde{\alpha} = 1.5\alpha$ (lower plots) (b). The underlying assumption is obviously that the $\tilde{\alpha}$ estimation feature of the proposed adaptive FL permits the tracking speed and flux errors, caused by the T_r variation, to be governed to zero at speed steady-state.

Fig. 13 (a) shows that for values of $\tilde{\alpha}$ provided to the FL controller lower than those of the real machine occurring for heating of the induced part track or for the modelled end-effect demagnetization higher than that of the real machine ($\hat{L}_r < L_r$), the speed tracking error increases significantly at high values of the load force and for low values of the LIM speed. At minimum speed (zero) and maximum load (80 N), the speed tracking error gets values about 30%. On the contrary, the flux tracking error increases significantly at high values of the load force and LIM speed. At maximum speed (5 m/s) and load (80 N), the speed tracking error gets values about 20%. The higher is the difference between the value of $\tilde{\alpha}$ provided to the FL controller and that of the real machine, the higher is the corresponding speed and flux tracking error, as expected. It means that when the induced part track increases its temperature because of heating, speed control becomes problematic at high load and low speed, while flux control becomes problematic at high load and high speed.

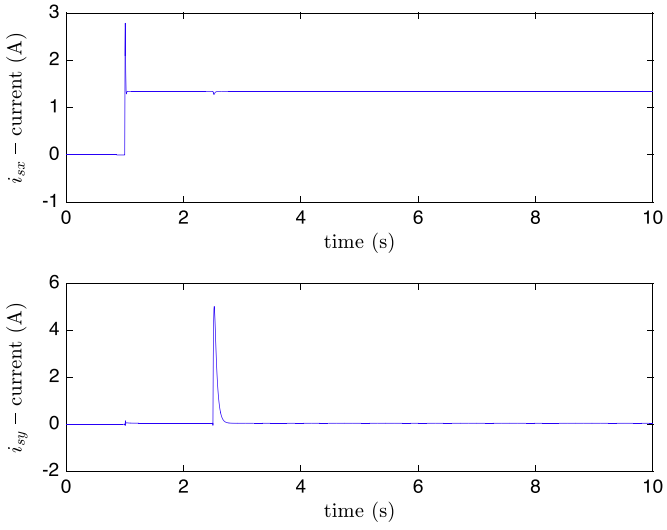

Fig. 11. i_{sx}, i_{sy} inductor currents with a flux step of 0.6 Wb at $t=1$ s, followed by a speed step $0 \rightarrow 0.2$ m/s at no load (simulation).

Fig. 13 (b) shows that for values of $\tilde{\alpha}$ provided to the FL controller higher than those of the real machine occurring for cooling of the induced part track or for the modelled end-effect demagnetization lower than that of the real machine ($\hat{L}_r > L_r$), the speed tracking error increases significantly at high values of the load while it presents a dependence of initial reduction and further increases at increasing LIM speeds presenting a minimum (depending from the detuning of T_r). At minimum speed (zero) and maximum load (80 N), the speed tracking error gets values about 15%. On the contrary, the flux tracking error presents a negligible dependence from the load force almost in the entire range of the LIM speed. Moreover, the flux tracking error decreases significantly at increasing values of the LIM speed with flux tracking error getting values about 30%.The higher is the difference between the value of $\tilde{\alpha}$ provided to the FL controller and that of the real machine, the higher is the corresponding speed and flux tracking error, as expected. It means that when the induced part track decreases its temperature because of cooling, speed control becomes problematic at high load and low speed, while flux control becomes problematic at low speeds, independently from the load.

In order to show the improvements achievable thanks to the adoption of the proposed adaptive FL in comparison with the non-adaptive FL, a further test has been provided. In particular Figs. 14 and 15 show a simulation test at 5 m/s and 0.6 Wb, with a load force of 80 N inserted at 3 s and removed at 7 s. This test is obtained with the adaptive FL, and the non-adaptive FL for $\tilde{\alpha} = 0.5\alpha$ and for $\tilde{\alpha} = 1.5\alpha$. Obviously the non-adaptive FL behaves as the adaptive FL when the induced part time constant is perfectly known, $\tilde{\alpha} = \alpha$. So, the aim of this test is to show the effectiveness of the proposed approach when the induced part time constant is not perfectly known, as occurs in real cases. Such an effect is demonstrated by showing the deterioration of the dynamic performance of the traditional FL with respect to the adaptive one proposed here, whenever an incorrect knowledge of the parameter α occurs.

From this test the improvements achievable thanks to the adoption of the proposed approach is evident. In fact the adaptive FL allows us to track the speed and flux references with negligible errors, whereas for the non-adaptive FL the higher is the estimation error of the induced part time constant, the higher is the tracking error.

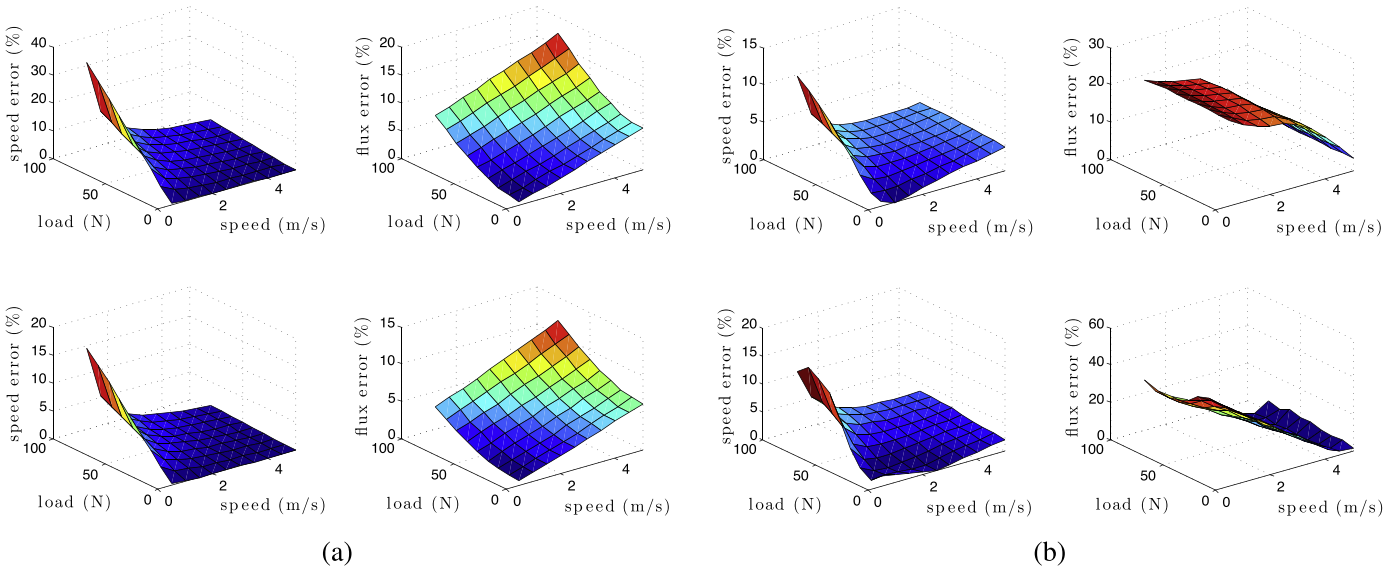

Fig. 13. Surfaces of the speed and flux tracking errors vs LIM speed and load force obtained with the non-adaptive FL for $\tilde{\alpha} = 0.5\alpha$ (upper plots) and $\tilde{\alpha} = 0.75\alpha$ (lower plots) (a); and for $\tilde{\alpha} = 1.25\alpha$ (upper plots) and $\tilde{\alpha} = 1.5\alpha$ (lower plots) (b).

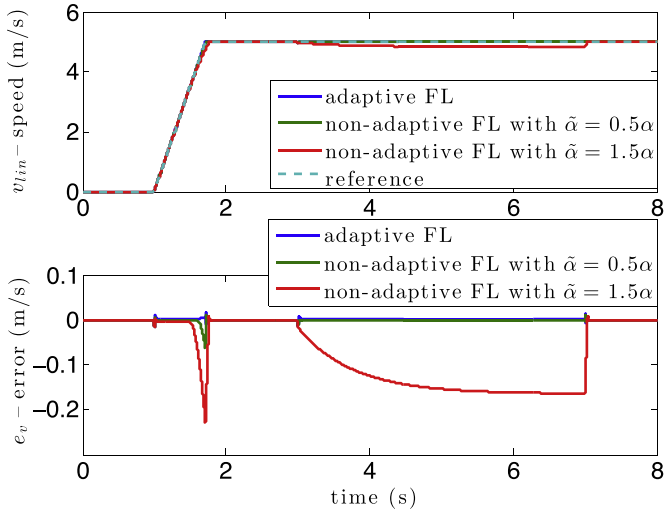

Fig. 14. Reference and measured speed (upper plot), tracking error (lower plot), during a test when the estimated $\tilde{\alpha}$ is detuned of $\pm 50\%$ (simulation).

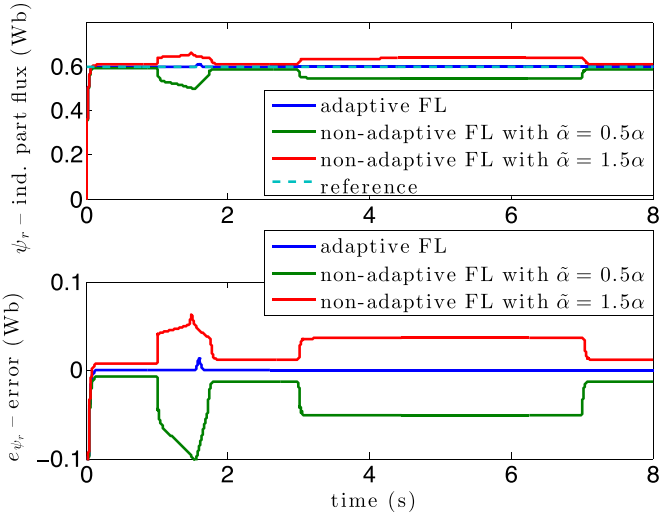

Fig. 15. Reference and measured flux (upper plot), tracking error (lower plot), during a test when the estimated $\tilde{\alpha}$ is detuned of $\pm 50\%$ (simulation).

5. Test set-up

A test setup has been suitably built to validate proposed FL control technique. The machine under test is a LIM model Baldor LMAC1607C23D99, whose rated data and electrical parameters are shown in Table 2. The LIM has been equipped with a linear encoder Numerik Jena LIA series. The LIM presents an induced part track on length 1.6 m. The employed test setup consists of:

- a three-phase linear induction motor with parameters shown in Table 2;
- a frequency converter which consists of a three-phase diode rectifier and a 7.5 kVA, three-phase VSI;
- a dSPACE card (DS1103) with a PowerPC 604e processor for fast floating-point calculation at 400 MHz, and a fixed-point DSP TMS320F240.

The test set-up is equipped also with a torque controlled PMSM model Emerson Unimotor HD 067UDB305BACRA mechanically coupled to the LIM by a pulley-strap system, to implement an active load for the LIM. Fig. 16 shows the test setup.

6. Experimental results

The experimental tests have been performed adopting the test set-up described in Section 5. The inverter has been driven, as in the simulated tests, by a SV-PWM, with the PWM frequency set at 5 kHz. The entire adaptive FL control system has been implemented on the DS-1103 board at the sampling frequency of 10 kHz. In the experimental test same condition of the simulation test shown in Figs. 9–12 has been considered in order to conveniently compare the obtained simulation results. The high speed test cannot be reproduced experimentally due to the limited length of the induced part track (1.6 m). In particular at $t=0$ s a step reference of the induced part flux of 0.6 Wb has been initially given to the drive. At $t=1.5$ s a speed step reference of 0.2 m/s has been given at no load. As in the simulated test, at the beginning,

Table 2
Parameters of the LIM.

Inductor resistance R_s (Ω)	11
Inductor inductance L_s (mH)	637.6
Induced part resistance R_r (Ω)	32.57
Induced part inductance L_r (mH)	757.8
3-phase magnetizing inductance L_m (mH)	517.5
Pole-pairs	3
Rated speed (m/s)	6.85
Mass (kg)	20

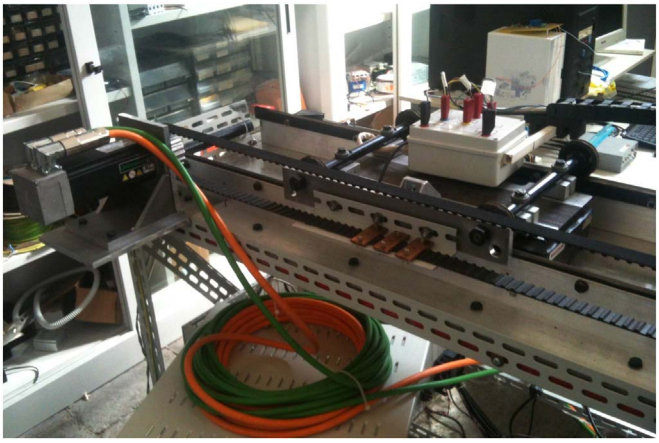

Fig. 16. Photograph of the experimental test setup.

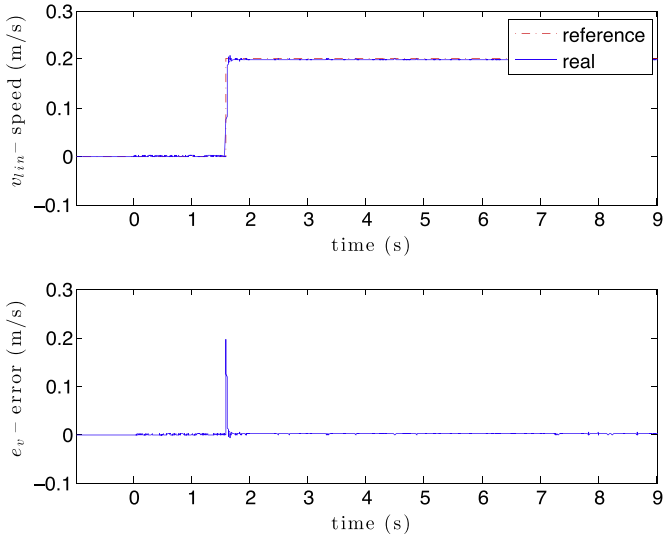

Fig. 17. Reference and real speed, speed tracking error with constant $v=0.2$ m/s, and $|\psi_r| = 0.6$ Wb (experimental).

the value of $\tilde{\alpha}$ provided to the FL controller is different from the value of the real machine (detuning of the FL controller).

Figs. 17–20 show the same kind of waveforms as plotted in the simulated tests, obtained under the above cited test. The same conclusion given for the simulation results can be given here. Indeed Fig. 20 clearly highlights the correct adaptation of the $\tilde{\alpha}$ firstly during the initial flux transient and secondly during the speed transient. At the end of the test, in a time interval of about 9 s, the value of $\tilde{\alpha}$ has been correctly estimated by the system. It should be minded that, exactly as in the simulated test, the real α of the LIM varies with its speed because of the end-effects. The speed waveform exhibits a very fast dynamics, even during the contemporary convergence process of $\tilde{\alpha}$. Even the $|\psi_r|$ waveform,

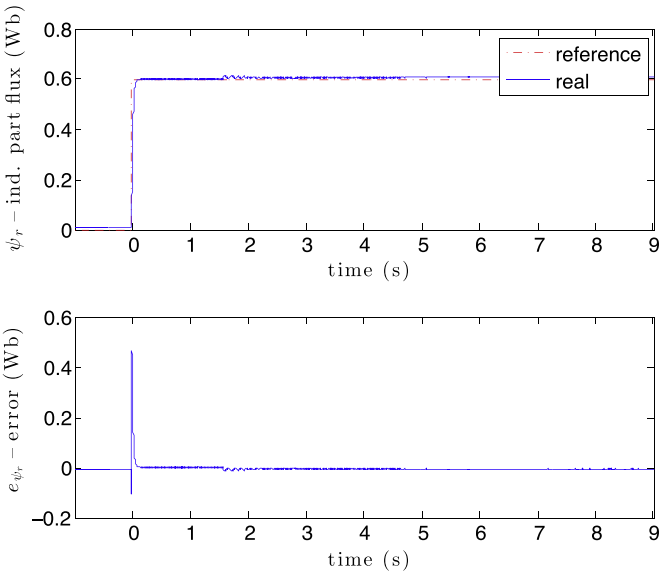

Fig. 18. Reference and real flux $|\psi_r|$, flux tracking error with constant $v=0.2$ m/s, and $|\psi_r| = 0.6$ (experimental).

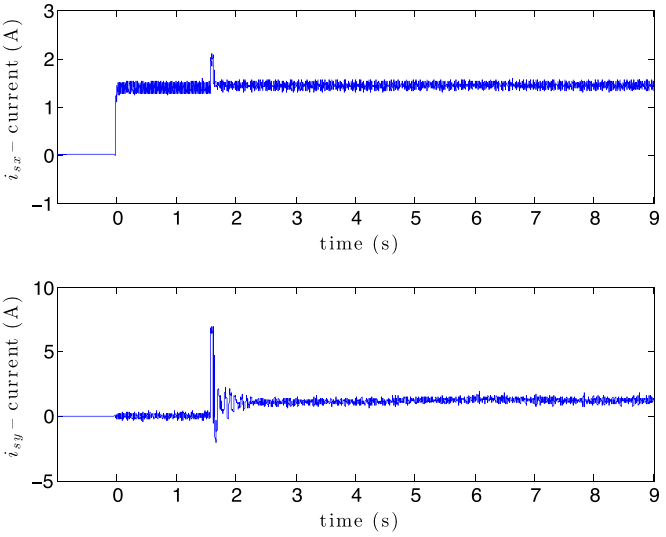

Fig. 19. i_{sx}, i_{sy} inductor currents with constant $v=0.2$ m/s, and $|\psi_r| = 0.6$ Wb (experimental).

shown in Fig. 18, correctly tracks its reference with zero steady-state tracking error, thanks to the on-line $\tilde{\alpha}$ estimation feature. Finally, the i_{sx}, i_{sy} waveforms, shown in Fig. 19, are coherent with the speed and flux waveforms, and with the simulation result. In particular, i_{sx} is maintained at a constant value. On the other hand, i_{sy} exhibits a step-wise waveform, which is proportional to the electromagnetic force. However, differently from the simulation results, here there is a non-null steady state value of the i_{sy}, this is due to the friction of the wheels and of the pulley-strap system.

7. Conclusion

This paper proposes an adaptive input–output feedback linearization technique for LIMs, taking into consideration the dynamic end-effects. As a main original content, however, this work proposes a new control law integrating an on-line estimation of the induced part time constant. The estimation law of the induced part time constant has been relieved thanks to a Lyapunov based

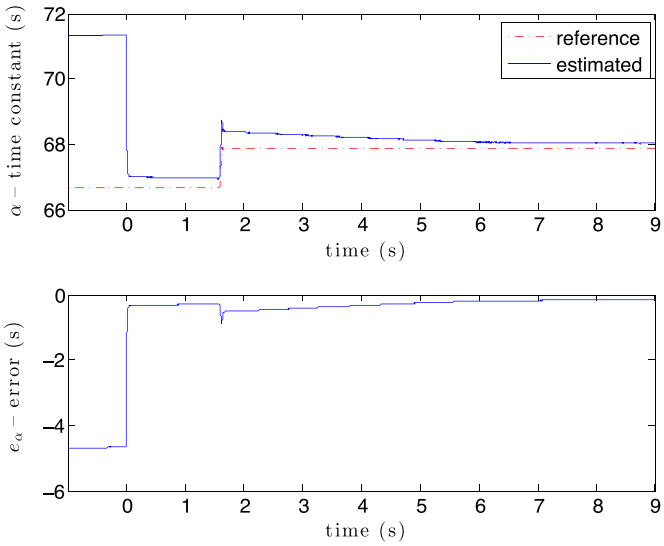

Fig. 20. Reference α and estimated $\tilde{\alpha}$, estimation tracking error with constant $v=0.2$ m/s, and $|\psi_f| = 0.6$ Wb (experimental).

analysis and thus the stability of the entire control law, including the adaptation algorithm, is intrinsically guaranteed. Moreover, with such an approach even the real on-line variation of the induced part time constant with the speed is retrieved, overcoming thus one of the limits of previously developed approaches where such a variation had been considered a priori known. The proposed technique, integrating the on-line induced part time constant estimation, has been tested in numerical simulations and experimentally on a suitably developed test set-up.

References

Alonge, F., Cirrincione, M., Pucci, M., & Sferlazza, A. (2015a). Input-output feedback linearizing control of linear induction motor taking into consideration the end-effects. Part I: *Theoretical analysis*. *Control Engineering Practice*, *36*(2), 133–141.

Alonge, F., Cirrincione, M., Pucci, M., & Sferlazza, A. (2015b). Input-output feedback linearizing control of linear induction motor taking into consideration the end-effects. Part II: *Simulation and experimental results*. *Control Engineering Practice*, *36*(2), 142–150.

Alonge, F., Cirrincione, M., Pucci, M., & Sferlazza, A. (2016). Input-output feedback linearization control with on-line MRAS based inductor resistance estimation of linear induction motors including the dynamic end-effects. *IEEE Transactions on Industry Applications*, *52*(1), 254–266.

Boldea, I., & Nasar, S. A. (1997). *Linear motion electromagnetic devices*. New York, USA: Taylor & Francis.

Boldea, I., & Nasar, S. A. (1999). Linear electric actuators and generators. *IEEE Transactions on Energy Conversion*, *14*(3), 712–717.

Da Silva, E. F., Dos Santos, E. B., Machado, P., & De Oliveira, M. (2003). Dynamic model for linear induction motors. In *2003 IEEE international conference on industrial technology* (Vol. 1, pp. 478–482). Maribor, Slovenia: IEEE.

De Luca, A., & Ulivi, G. (1989). Design of an exact nonlinear controller for induction motors. *IEEE Transactions on Automatic Control*, *34*(12), 1304–1307.

Duncan, J. (1983). Linear induction motor-equivalent-circuit model. In: *IEE Proceedings B (Electric Power Applications)* (Vol. 130, pp. 51–57). IET.

Huang, C. -I., & Fu, L. -C. (2003). Passivity based control of the double inverted pendulum driven by a linear induction motor. In *2003 IEEE international conference on control applications* (Vol. 2, pp. 797–802). Istanbul, Turkey: IEEE.

Isidori, A. (1995). *Nonlinear control systems* (3rd edition). London, UK: Springer.

Khalil, H. K. (2002). *Nonlinear systems*. Englewood Cliffs, New Jersey, USA: Prentice Hall.

Kim, D.-I., Ha, I.-J., & Ko, M.-S. (1990). Control of induction motors via feedback linearization with input-output decoupling. *International Journal of Control*, *51*(4), 863–883.

Krzeminski, Z. (1987). Nonlinear control of induction motor. In: *10th IFAC World congress* (Vol. 349, p. 33).

Laithwaite, E. R. (1975). Linear electric machines—A personal view. *Proceedings of the IEEE*, *63*(2), 250–290.

Landau, I. D., Lozano, R. M'Saad, M., & Karimi, A. (2011). *Adaptive control: Algorithms, analysis and applications*. London, UK: Springer Science & Business Media.

Leonhard, W. (2001). *Control of electrical drives*. Berlin, Heidelberg: Springer.

Lin, F.-J., & Wai, R.-J. (2001). Hybrid control using recurrent fuzzy neural network for linear induction motor servo drive. *IEEE Transactions on Fuzzy Systems*, *9*(1), 102–115.

Lin, F.-J., & Wai, R.-J. (2002). Robust control using neural network uncertainty observer for linear induction motor servo drive. *IEEE Transactions on Power Electronics*, *17*(2), 241–254.

Marino, R., Peresada, S., & Valigi, P. (1993). Adaptive input–output linearizing control of induction motors. *IEEE Transactions on Automatic Control*, *38*(2), 208–221.

Marino, R., Tomei, P., & Verrelli, C. M. (2010). *Induction motor control design*. London, UK: Springer.

Nasar, S. A., & Boldea, I. (1987). *Linear electric motors: Theory, design, and practical application*. Englewood Cliffs, New Jersey, USA: Prentice-Hall inc.

Poloujadoff, M. (1980). *The theory of linear induction machinery*. Oxford, UK: Clarendon Press.

Pucci, M. (2012). Direct field oriented control of linear induction motors. *Electric Power Systems Research*, *89*, 11–22.

Pucci, M. (2014). State space-vector model of linear induction motors. *IEEE Transactions on Industry Applications*, *50*(1), 195–207.

Slotine, J.-J. E., & Li, W. (1991). *Applied nonlinear control*. New Jersey: Prentice hall.

Vas, P. (1998). *Sensorless vector and direct torque control*. Oxford, UK: Oxford University Press.

Wai, R.-J., & Chu, C.-C. (2007). Robust petri fuzzy-neural-network control for linear induction motor drive. *IEEE Transactions on Industrial Electronics*, *54*(1), 177–189.

Yamamura, S. (1979). *Theory of linear induction motors*. New York, USA: John Wiley & Sons Inc.